Molecular Dynamics Simulation of the Water/2-Heptanone Liquid-Liquid Interface

Pedro Alexandrino Fernandes, M. Natália D. S. Cordeiro, and José A. N. F. Gomes*

CEQUP/Departamento de Química, Faculdade de Ciências da Universidade do Porto, Rua do Campo Alegre 687, 4150 Porto, Portugal

Received: November 12, 1998; In Final Form: April 20, 1999

Molecular dynamics simulations were performed to study the structural and dynamic properties of the water/2-heptanone (HPT2) liquid/liquid interface. It was found that HPT2 forms a bilayer structure at the interface, pointing its polar heads into the aqueous phase. Water molecules penetrate the hydrophilic headgroup region but not the hydrophobic core. At the hydrophilic region water molecules establish hydrogen bonds with the ketone oxygen of the HPT2 molecule. Behind that zone, the water molecules show a preference in keeping their dipoles in the interfacial plane and these orientations remain in two or three molecular layers. The water dipole distribution is slightly asymmetric, having an average excess in the resulting component normal to the interfacial plane. The water dipoles point toward the aqueous phase for waters in the aqueous side of the interface and into the organic phase for water molecules in the organic side of the interface. The water structure remains almost unchanged at the Gibbs dividing surface. The HPT2 structure is not so robust, and near the interface it is distorted by the presence of the aqueous phase. Self diffusion exhibits long range anisotropy, diffusion toward the interface being slower than diffusion in the interfacial plane. The water orientational dynamics is slowed down near the interface. The HPT2 reorientation becomes anisotropic at the interface as reorientations perpendicular to the interface are slower than those in the interfacial plane. The interface was found to be sharp, highly corrugated, and broadened by capillary waves.

I. Introduction

The comprehension of charge transfer mechanisms across the interface between immiscible liquids is fundamental to many areas of chemistry, physics, and biology. Examples include ion transport in biological membranes,[1] drug delivery in pharmacology,[2] phase transfer catalysis,[3] and kinetics of ion extraction.[4] Central to the interpretation of experimental data has been the correct description of the structure and dynamics of the neat interface. Despite its importance, our knowledge about interfacial properties is still very limited, both experimentally and theoretically. Until a few years ago, technical difficulties prohibited experimental probing at the molecular level. At the same time, theoretical studies have been restricted to continuum approaches[5,6] because of the problem's complexity.

Recently the situation has improved significantly. Experimentally, second-harmonic generation and sum frequency generation techniques[7−11] enabled direct measurement of microscopic properties at the interfacial region. Theoretically, the improvement of computational resources and the use of methods, such as Monte Carlo or molecular dynamics simulations, allowed the estimation of molecular interfacial properties, such as density profiles, surface roughness, or specific solvent orientation.[12−16]

In this work we will focus on the properties of the water/2-heptanone (HPT2) liquid/liquid interface. It has been recently demonstrated that HPT2 can be used to carry out two-phase electrochemistry, and simple and assisted ion transfers between these two solvents were already performed.[17,18]

In fact, HPT2 has a low toxicity as it is nonaromatic and not halogenated and may thus be applied in large scale industrial processes. Other solvents, such as acetophenone, 1,2-dichloroethane, and nitrobenzene although still widely used, have a much higher toxicity.

In this paper the water/HPT2 liquid/liquid interface is studied using molecular dynamics simulations because this method was proved to be very useful in achieving the microscopic interfacial characterization.[12−16]

The solubility of water in HPT2 (1.41% (w/w)) is too large to be ignored, and thus, the simulated system will consist in hydrated HPT2 and water. Earlier workers found no need to take mutual solubility into account because it is usually very small. This is also the case for the solubility of HPT2 in water (0.43% (w/w)), which corresponds to a ratio of 1 HPT2 molecule:1640 water molecules. This is too small to be considered in our system.

The present study was preceded by a series of pure and hydrated HPT2 molecular dynamics simulations[19] where several intermolecular potentials were tested against experimental data.

This paper is organized as follows. The water and HPT2 molecular models, the potential functions, and the details of the simulations are outlined in the next section. Section III presents the results obtained in this study. Structural and dynamic properties of both solvents near and across the interface are discussed, together with an analysis of the interface structure and dynamics. In section IV a picture of the properties of our interfacial system is drawn, based on the results reported in previous sections.

II. Computational Model

A. Molecular Models and Potentials. Each HPT2 molecule was represented by eight interaction sites as depicted in Figure 1. Notice that united atom models were used for the CH_n (n = 2 or 3) groups with interaction sites located on the corresponding carbon atoms.

* Corresponding author.

10.1021/jp9844213 CCC: $18.00
Published on Web 07/13/1999

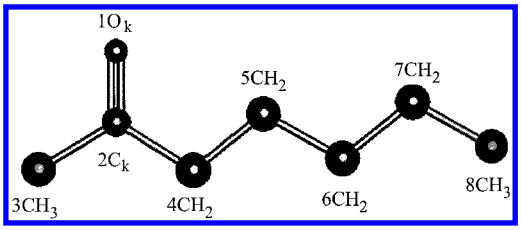

Figure 1. Schematic representation of the model used for each HPT2 molecule.

Figure 1 shows a schematic representation of the HPT2 molecular model, together with the group notation that will be used throughout this paper. For water the well-known SPC/E model[20] was adopted.

The intermolecular potentials used in this work for the HPT2−HPT2 and HPT2−H_2O interactions have been reported previously.[19] Specifically, they are pairwise additive potentials that include Coulombic and Lennard-Jones (LJ) terms. For the HPT2 molecule, the LJ parameters are those of the OPLS force field[21] and the coulombic parameters are based on charges derived from ab initio calculations (see ref 19 for details). For the interaction potential between HPT2 and H_2O, standard combination rules have been used.

The potential parameters for the intramolecular interactions in the HPT2 molecule were taken from the CHARMm force field.[22] These describe the flexible bonds, angles, and dihedrals, as well as an improper dihedral used to maintain the planarity of the sp^2 carbonyl carbon.

The water molecules were considered rigid. This procedure allows us to increase the time step used to 1.0 fs, and as previously checked, this increase has no influence in the results obtained. The absence of coupling between water stretching and bending and other vibrations in our system justifies this procedure.

B. Method. The system consisted initially on two separate boxes, one containing 794 water molecules and the other a mixture of 168 HPT2 molecules with 15 water molecules, to obtain the experimental concentration of water in saturated HPT2. The initial cross section of both boxes was 25 × 25 Å with a length selected to give the density of the pure liquids (0.997 g/cm^3 for water and 0.8124 g/cm^3 for HPT2).

All simulations were performed in the NPT ensemble because it is very important to allow for volume variations. In fact, the density of the interfacial zone is a priori unknown, and to impose a fixed initial volume can induce constraints in the formation of the interface, therefore affecting its structure and extension.

Both systems were first equilibrated during 300 ps, which guarantees that all energetic properties and their volumes and pressures were stabilized and oscillating around their mean values. The two boxes were then joined in one single box with the same cross section. Then the water phase was centered in the box by performing a translation in the *z* direction and applying the periodic boundary conditions (see Figure 2). After joining the two boxes, a first equilibration run of 5 ps was performed. In the beginning of that simulation the intermolecular potentials for the interactions between molecules belonging initially to different boxes were scaled by a factor of 10^{-9}. This scaling factor was increased afterward during 10 sequential runs, each by 0.5 ps. With this procedure the interaction potentials reached their final values at the end of the run. A new equilibration of 150 ps in the NPT ensemble was found to be enough to equilibrate this new system according to the same criteria as referred before.

In order to better explore the configurational space and check the dependence of results on the initial conditions, the procedure described above was repeated three times more, starting always from independent configurations of water and saturated HPT2. In this way, four independent simulation boxes were obtained, each one with two interfaces perpendicular to the *z* axis (by convention), as depicted in Figure 2.

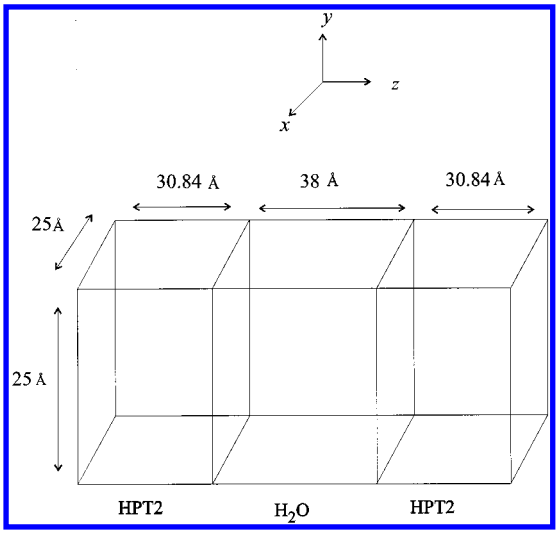

Figure 2. Schematic picture of the box used in the simulations.

Four 300 ps simulations were performed with each box for data collection. The Nosé-Hoover thermostat and barostat[23,24] were used in all simulations. Temperature and pressure were kept at 300 K and 1 bar, respectively.

The integration of the equations of motion was performed using a Verlet leapfrog algorithm, with a time step of 1 fs. Cutoffs of 10 and 12 Å were applied for the short and long range interactions. A multiple time step algorithm[25] was used to evaluate interactions for distances larger than 10 Å, with a frequency of actualization of 10 fs. It was checked that this technique would lead to good energy conservation (without the use of a thermostat) and would not affect the properties of the system.

Periodic boundary conditions were applied in all three directions. An Ewald summation method with tinfoil boundary conditions was used to deal with the long range forces. It is important to note that this method will produce the replication of the interfaces in the *z* direction. Thus, a water molecule in the central box will interact with water (and not with HPT2) at average *z* distances in the interval (approached to integer distances) [81 Å + 100*k* Å, 119 Å + 100*k* Å], where *k* is a nonnegative integer (see Figure 2). We considered this effect to be negligible due to the distance considered, and not capable of distorting the structural properties of the system, because it acts almost equivalently in close molecules. So this approximation seems to be better than using switching or shifting methods to deal with long range forces. When a box with two interfaces is used, care must be taken to prevent them from interacting. In those cases the simulation box must be long enough to ensure the independence between both interfaces. In our system the initial separation between both interfaces was 38 Å along the water phase and 61.68 Å along the organic phase, i.e., 3.2 and 5.2 times greater than the long range cutoff distance what seems quite enough to avoid interfacial correlations.

III. Results

A. Density Profiles. The average density profile along the interface normal (*z* distance) is shown in Figure 3. The profile was calculated using slabs of thickness 1 Å parallel to the interfacial plane.

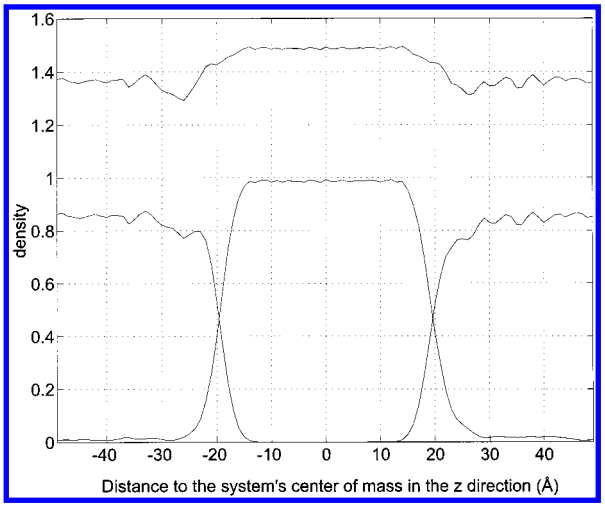

Figure 3. Average density profile for the water|HPT2 system. The upper line represents the total density of the system, translated vertically by +0.5. The two Gibbs dividing surfaces are located at +19.4 and −19.4 Å.

During the MD simulation the interface may change its position due to the build-up of translational motion. This would cause an artificial smoothing of the density profile and an erroneous enlargement of the density decay length at the interfacial zone. This effect would be emphasized when accumulating density profiles from independent simulations. In order to overcome this artifact, the *z* distance shown in Figure 3 is measured in relation to the center of mass of each box. The profile presented (as all results in this paper) is an average of the four simulations performed. During the course of the simulations, we monitored the *z* coordinate of the center of mass and we found small fluctuations around its mean value (standard deviation of the mean = 0.24 Å). The average density profiles show two stable interfaces, indicating that the potential models describe successfully the formation of the interfaces. The mass percentage of water in HPT2 is stable and homogeneously distributed, with an average value of 1.57% (w/w) which is very close to the experimental value.

If we define $Z^{1/2}_{H_2O}$ as the *z* coordinate value where $\rho_{H_2O}(z) = {}^1/_2\rho^{bulk}_{H_2O}$, and in a similar way $Z^{1/2}_{HPT2}$, we can locate the Gibbs dividing surface as the middle point between $Z^{1/2}_{H_2O}$ and $Z^{1/2}_{HPT2}$ (which were almost coincident). From Figure 3 we can locate the two Gibbs dividing surfaces at ±19.4 Å.

There are, in principle, two extremal molecular arrangements that may generate a gradual decrease of the concentration perpendicular to the interfacial surface. One extreme is characterized by a sharp transition from one phase to another, and the interface position fluctuates with time due to thermal motion (capillary waves). The other extreme consists in a gradual change in the composition of the system, from one bulk phase to the other, and that corresponds to a maximum of the interfacial width. Density profiles alone do not clarify at what point between these two extremes lies our system. More detailed information can be obtained by defining the positions and widths of local interfaces.

B. Interfacial Width and Position. One approach to better characterize the interfacial density fluctuations is to define a local interface. The method described below has been used by other workers[12−16] and is derived from the procedure developed by Weeks[26,27] to define a capillary wave Hamiltonian.

The interfacial plane was divided into $N \times N$ squares and, for each saved configuration (saving frequency = 25^{-1} fs), all the molecules in the *ij* partial box of cross section S/N^2 (*S* being the total interfacial area) were taken into account). Local surface locations H_{ij} and widths W_{ij} may in this way be defined as

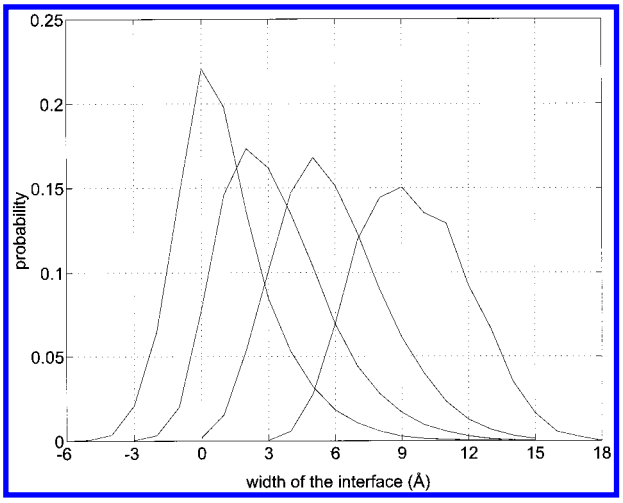

Figure 4. Probability distribution of the width of the interface calculated using different surface areas. The lines correspond, from left to right, to $N = 4$, 3, 2, and 1, respectively.

$$H^{left,right}_{ij} = {}^1/_2\,(h^{left,right}_{ij}\,(H_2O) + h^{left,right}_{ij}\,(HPT2)) \quad (1)$$

$$W^{left}_{ij} = h^{left}_{ij}\,(HPT2) - h^{left}_{ij}\,(H_2O) \quad (2)$$

$$W^{right}_{ij} = h^{right}_{ij}\,(H_2O) - h^{right}_{ij}\,(HPT2) \quad (3)$$

To define $h_{ij}(H_2O)$ for each saved configuration the mass fraction of water as a function of the *z* coordinate, $\chi_m(z)$ is estimated according to

$$\chi_m(z) = \frac{\rho_{H_2O}(z)}{\rho_{H_2O}(z) + \rho_{HPT2}(z)} \quad (4)$$

and $h_{ij}(H_2O)$ is then considered as the first *z* coordinate where $\chi_m(z) \le \chi^{bulkHPT2}_m$, when monitored from bulk water to bulk HPT2. This method locates the water interface where its solubility lies at or below its average solubility in bulk HPT2.

$h_{ij}(HPT2)$ is simply defined as the *z* location of the HPT2 site most advanced into the water phase

$$hij^{left}\,(HPT2) = \max(z_{HPT2}), \quad z < 0 \quad (5)$$

$$hij^{right}\,(HPT2) = \min(z_{HPT2}), \quad z > 0 \quad (6)$$

where z_{HPT2} corresponds to the *z* coordinate of the sites of the HPT2 molecules. Figure 4 shows the interface width distributions obtained using N = 1, 2, 3, and 4, respectively. Note that data coming from both interfaces was accumulated. The average widths of the distributions presented in Figure 4 are 9.3, 5.6, 3.2, and 1.0 Å when *N* increases from 1−4. $N > 4$ would result in a square with sides smaller than a single HPT2 molecule, and the location of the interface in successive squares would not be independent.

The successive shift of the distributions toward smaller values indicates that the widths obtained with the large surface areas may correspond to surface shape deformations instead of interpenetrations. The magnitudes obtained for the average widths give us a picture of a sharp interface without significant mixing. Notice that *if* there was a continuous and gradual change in composition, from one bulk phase to the other, the width

distributions should be all centered at the same large positive value, i.e., at a distance over which composition changes from pure water to saturated HTP2. A similar behavior was also observed in other interfacial systems,[12,14−16] although the average width of all of them was found to be negative for the smaller surface areas. The positive value obtained here for $N = 4$ reflects the greater hydrophilicity of HPT2 in relation to other organic solvents used in the simulation of liquid−liquid interfaces.[12,14−16]

Figure 5 shows the distributions for the interface position calculated using different surface areas. In order to allow for the accumulation of data from both interfaces, we do not show the absolute interface positions, but instead, we showed the deviations of the position of the interface in relation to its average.

We can observe a monotonous broadening of the distributions with decreasing surface area, from the highest and sharpest peak (corresponding to $N = 1$) to the lowest and broadest peak (corresponding to $N = 4$). If the interface was flat, this distribution should be independent of N. The monotonous broadening of the position fluctuations with decreasing surface areas give us a picture of a highly corrugated interface, with local penetrations that can reach up to 10 Å. This data is consistent with a sharp interface broadened by capillary waves.

Thermodynamics can be used to relate the surface tension of the interface (γ_c) with the interfacial width arising from the thermal fluctuations superimposed under an infinitely sharp surface.[26] From the capillary wave theory this relation is given by

$$\langle \zeta^2 \rangle = \frac{k_B T}{4\pi\gamma_c} \ln\left[\frac{1 + 2(\pi a/l)^2}{1 + 2(\pi a/L)^2}\right] \quad (7)$$

In this equation, L and l are the upper and lower cutoffs of the capillary wave spectrum, respectively, $\langle \zeta^2 \rangle$ is the mean square fluctuation of the surface location away from its equilibrium position, and a depends upon the density difference across the interface and gravity. $a^2 = 2\gamma_c/mg(\rho_l - \rho_g)$, ρ_l and ρ_g being the liquid and gaseous number densities and m the mass of the molecule. The short range cutoff is usually taken as the molecular diameter, and the long range cutoff L is determined by the system size. Since the effect of gravity has not been included in the present work, as it is common practice in liquid−liquid interface simulations, eq 7 simplifies to

$$\langle \zeta^2 \rangle = \frac{k_B T}{2\pi\gamma_c} \ln\left[\frac{L}{l}\right] \quad (8)$$

Using the mean square deviation of the surface position distribution obtained with $N = 4$ and $l = 6.4$ Å, we obtain $\gamma_c = 12.9 \pm 0.1$ dyn/cm. l was chosen to be the average length of the interfacial HPT2, although γ_c is not very sensitive to it.

When we increase the area of the interface we are increasing the number of molecules of both liquids in close contact. Because the interactions inside each liquid are thermodynamically more favorable than the interactions between different liquids (the reason for immiscibility), the amplitude of the variations in the interfacial area becomes closely related to the balance between those two types of interactions. So, the higher the hydrophobicity of the organic liquid the greater the amount of work necessary to increase the area of close contact with water. As far as we know there is no experimental value for the surface tension of the water/HPT2 interface. However, experimental and calculated surface tensions of other interfacial systems have been reported in literature. An experimental value

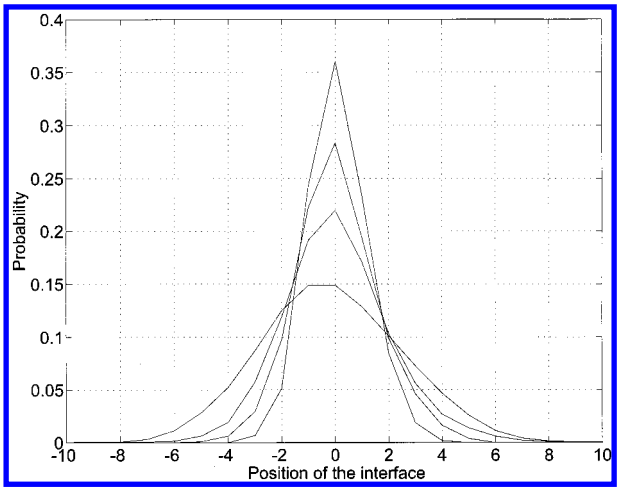

Figure 5. Probability distributions for the fluctuations of the position of the interface calculated for different interfacial areas. The four lines correspond, from the sharpest to the broadest, to $N = 1$, 2, 3, and 4, respectively.

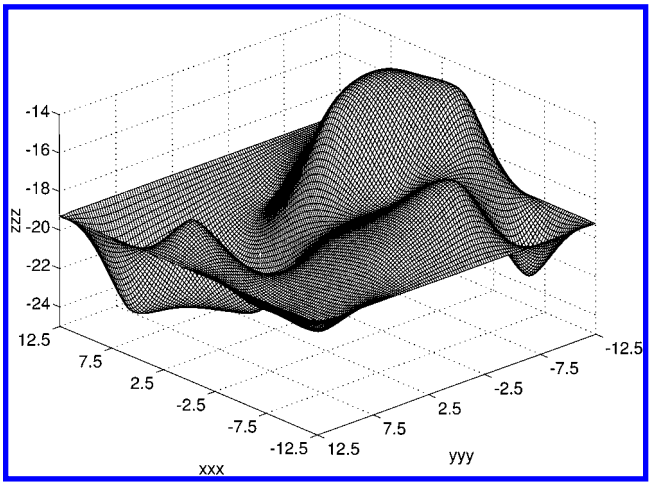

Figure 6. Snapshot of the Gibbs dividing surface, obtained by interpolation of the points corresponding to the position of the sixteen local interfaces obtained with the interface divided into 4 × 4 squares.

of 35 dyn/cm was reported for the water/benzene interface[12] and a value of 29 dyn/cm for the water/DCE interface[14] which is less hydrophobic than benzene.

The lower value obtained for the water/HPT2 interface may be due to the much higher hydrophilicity of HPT2 in comparison with the other organic liquids, and it is in qualitative agreement with the surface tensions of other liquid−liquid interfaces.

An interesting evidence of the effect of hydrophilicity in reducing the surface tension of a liquid−liquid interface can be drawn by analyzing some experimental results. In ref 28 a surface tension of 50.8 and 8.5 dyn/cm was reported for the water/*n*-octane and water/*n*-octyl alcohol liquid/liquid interfaces, respectively. Such a decrease on the interfacial surface tension may be associated to the much higher hydrophilicity of *n*-octyl alcohol in relation to *n*-octane, caused by the strong interactions (hydrogen bonds) between water and the hydroxyl group of alcohol. This situation is quite similar to the water−HPT2 interaction, as will be seen below.

Figure 6 depicts a snapshot of the interfacial surface. To define it we have used the location of the interface in each of the 4 × 4 squares and interpolated the surface only between these sixteen points. The part of the surface between the outer points and the cell boundaries (a border of 3 Å thickness) was forced to converge to the average position of the interface in

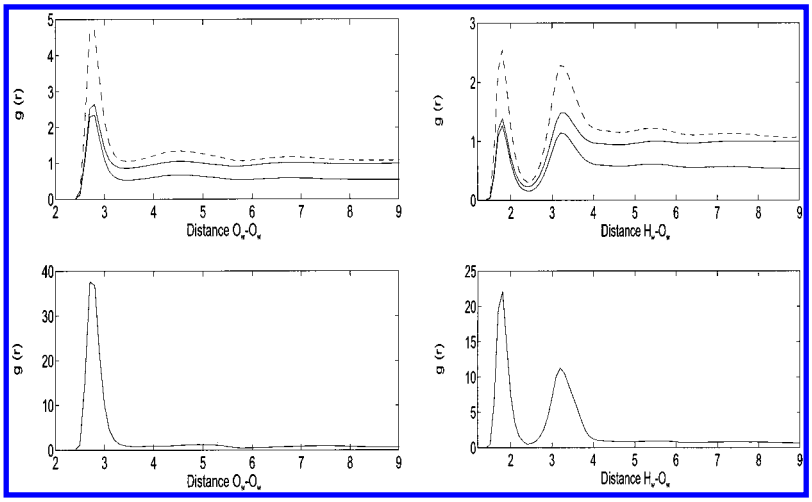

Figure 7. The left figures correspond to the O_w-O_w RDFs, and the right figures correspond to the H_w-O_w RDFs. In the top figures, the upper solid lines correspond to the RDFs in bulk water, the lower solid lines represent the RDFs calculated at the interface and normalized by the bulk water density, and the dashed lines depict the interfacial RDFs normalized by the interfacial water density. The bottom figures correspond to RDFs calculated in bulk HPT2.

that moment. This procedure was adopted because it makes the three dimensional visualization of the surface much more clear. This picture should be regarded as illustrative of the corrugations (capillary waves) that broaden the interfacial surface.

C. Structure. The structure of the H_2O and HPT2 can be described by the usual pair correlation functions and orientational distributions functions. In the following section, we will analyze the structure of each liquid from bulk phase to the interface (to bulk HTP2, in the case of water) and examine the preferred arrangements between H_2O and the HPT2 molecules.

1. Water Structure. The possible structural changes in water when changing from bulk phase to the interface can be studied in terms of atomic radial distribution functions (RDFs). The bulk RDFs were computed taking as the origin all the atoms between the planes $Z = \pm 4$ Å. Interfacial RDFs were estimated using as the origin all atoms between the planes $Z = \bar{z} \pm 2$ Å, where $\bar{z}$ represents the average position of the interface. There are two slabs to collect interfacial data, each one centered at the $\bar{z}$ of each interface. The bulk HPT2 region was considered to be the zone where $z \leq -38$ Å or $z \geq 38$ Å.

Figure 7 depicts the O_w-O_w and H_w-O_w RDFs in bulk water at the interface and in bulk HPT2. Inspection of this figure allows the following conclusions: (i) the location of the peaks is almost unaffected when passing from bulk water to bulk HPT2, (ii) the height of the peaks increases from bulk water to bulk HPT2, (iii) the first peak of bulk and interfacial water have almost the same height when equally normalized. This means that water basically keeps its structure almost unchanged at the interface, the differences being almost all due to the smaller number of water molecules outside the first coordination shell.

Integration of the first peaks of the O_w-O_w RDF results in a average coordination number of 5.2 in bulk water and 4.2 at the interface. Water in bulk HPT2 also keeps the first solvation shell with a similar structure, although the average coordination number decreases drastically due to the much lower density of water. Integration of the first peak results in a average of 0.7 neighbors.

2. Hydrogen-Bonding Analysis. To get some insight into the structural changes in water we performed a statistic analysis of the hydrogen bonding along the *z* axis. Two water molecules are considered to be hydrogen bonded if their pair interaction energy is less than −2.4 kcal/mol. Another criterion that is frequently used is to consider pair of water molecules that have

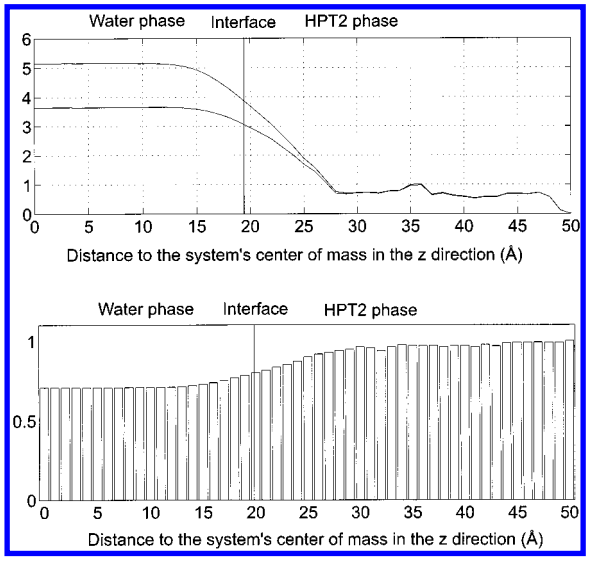

Figure 8. Top: Average coordination number of water (upper line) and average number of hydrogen bonds per water molecule (lower line), as a function of the distance to the interface. Bottom: The fraction of water molecules inside the first coordination shell that are hydrogen bonded. To achieve more accurate statistics, the results obtained from each half of the box were accumulated.

O−H distances inferior to the H_w-O_w RDF first minimum (2.4 Å). Both criteria give similar results and present the same dependence on the distance of the water molecules from the interface. The results presented here were obtained using the distance criterion. We also computed the number of neighbors in the water first coordination shell. All molecules for which the O_w-O_w distance was inferior to the O_w-O_w RDF first minimum (3.5 Å) were considered to belong to the first water solvation shell.

Figure 8 shows the average number of neighbors in the water first coordination shell, the total number of hydrogen bonds per water molecule, and the fraction of water molecules inside the first solvation shell that are hydrogen bonded. As can be clearly seen, the number of hydrogen bonds and the average coordination number decreases from bulk water to bulk HPT2, reflecting the decrease in the water density, although the number of hydrogen bonds only decreases significantly after the Gibbs dividing surface. The fraction of water molecules that are hydrogen bonded is not very strongly affected until past the

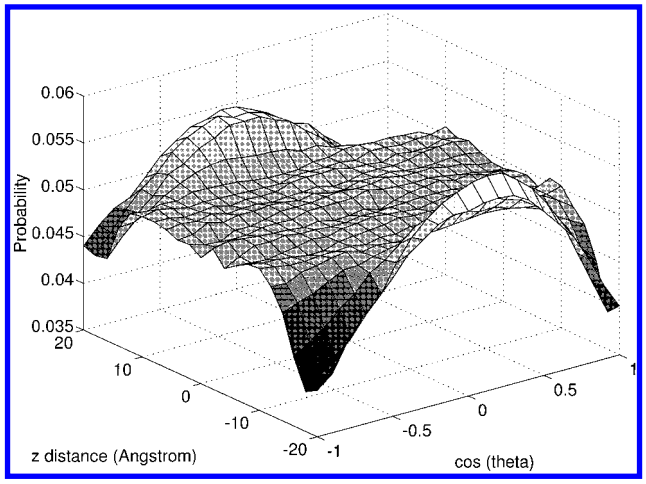

Figure 9. Probability distribution of the cosine of the angle theta as a function of the distance to the interface. θ represents the angle between the water dipole and the interface normal.

Gibbs dividing surface (which is consistent with the conservation of the water structure near the interface). Past the interface, the fraction of hydrogen bonds increases slowly along the first 10 Å into the HPT2 phase, after which almost all coordinated water molecules are hydrogen bonded. Similar behavior has been reported for other liquid−liquid interfacial systems.[12,14−16]

Our interpretation is that the water tends to keep its structure until reaching the Gibbs dividing surface. After passing it, water clusters tend to desegregate, because of the interactions with HPT2 molecules and to the reduced density of water in HPT2, which hinder spontaneous water associations. The first (the most probable) water molecules to become separated are the less tightly bonded, the ones which are not hydrogen bonded; this causes the observed increase in the fraction of hydrogen bonded molecules as we progress into the organic phase. In bulk HPT2 very few molecules can remain associated without being hydrogen bonded.

3. Water Orientational Structure. The results discussed in the last sections show how resistant is the water structure to changes introduced by the presence of the interface. Most significant changes occur only in the organic side of the interface and are due simply to the reduced number of water molecules. However, more pronounced interfacial effects can be detected analyzing the orientation of the water molecules.

Figure 9 shows the probability distribution for the angle between the water dipole moment and the interface normal. In bulk water there are no preferred orientations, as should be expected for a isotropic fluid. At the Gibbs dividing surface there is a significant tendency of the water molecules to have their dipole moments parallel to the interface rather than in the *z* direction, in clear agreement with the prediction given by the electrostatic continuum theories. This preferential dipolar orientation extends towards the bulk region for two or three molecular layers.

The distribution is slightly asymmetric, resulting in a excess on the average net *z* component of the water dipole moment near the interface.

Figure 10 shows the average *z* component of the water dipole moment per molecule $\langle \vec{\mu}_z \rangle$ normalized by the SPC/E water dipole moment, as a function of the distance to the center of mass of the system. The resulting $\langle \vec{\mu}_z \rangle$ points toward the aqueous phase in the aqueous side of the interface, as observed in the water liquid/vapor interface[29] and never exceeds the value corresponding to an isotropic orientation by more than 2%. On the organic side of the interface, the average dipole orientation

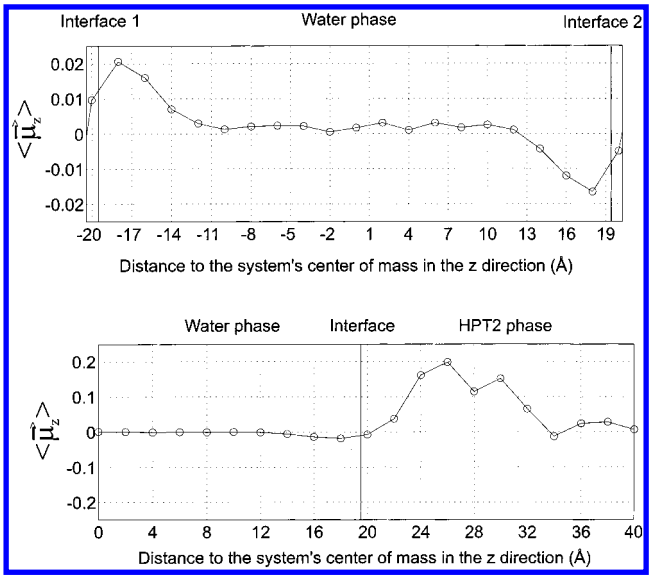

Figure 10. Average *z* component of the water dipole moment as a function of the distance to the interface until the Gibbs dividing surface (top) and across the total length of the box (bottom). System symmetry was used in order to obtain better statistics in bulk HPT2 zone, where only (on average) 15 water molecules exist. $\langle \vec{\mu}_z \rangle$ for $z > 0$ was accumulated with $-\langle \vec{\mu}_z \rangle$ for $z < 0$.

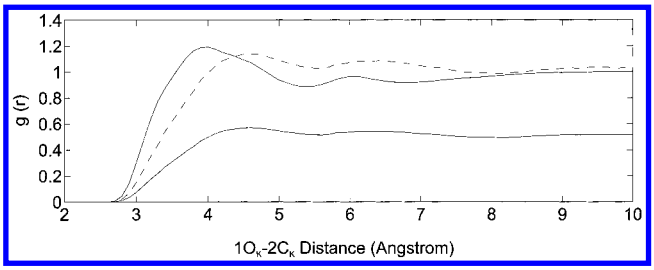

Figure 11. RDF for the $1O_k-2C_k$ associations. The upper solid line corresponds to the RDF calculated in bulk HPT2. The lower solid line and the dashed line corresponds to interfacial RDFs, normalized, respectively, by the bulk and interfacial densities.

reverses, pointing into the organic phase, favoring the establishment of hydrogen bonds between the water hydrogens and the ketone oxygens. This last orientation is more pronounced and results in a maximum $\langle \vec{\mu}_z \rangle$ 20% above the isotropic orientation. The *x* and *y* components of the average net water dipole moment are null, all over the simulation box, within statistical uncertainty. The same is true for its *z* component in bulk HPT2.

4. HPT2 Structure. The method of calculation of the $1O_k-2C_k$, $4CH_2-5CH_2$, and $8CH_3-8CH_3$ RDFs for HPT2 as a function of the distance from the interface is identical to that used for the water RDFs. The RDFs are also normalized taking into account the bulk and interfacial densities. The results obtained in the bulk region are equivalent to the ones obtained in independent simulations of saturated HPT2. The solid lines in Figure 11 correspond to the RDFs calculated in the bulk region and at the interface, normalized by the bulk density. Dashed lines correspond to the interfacial RDFs normalized by the interfacial density.

The $4CH_2-5CH_2$ and $8CH_3-8CH_3$ RDFs keep the location of their peaks at the interface. The only difference is on the coordination numbers that decrease to one half, because of the lower density of HPT2 at the interface (precisely to one half its bulk value). When normalized by the interfacial density the RDFs became very close to the bulk calculations. We conclude that those RDFs show the tendency of HPT2 to keep its bulk geometric structure near the interface, although with only one

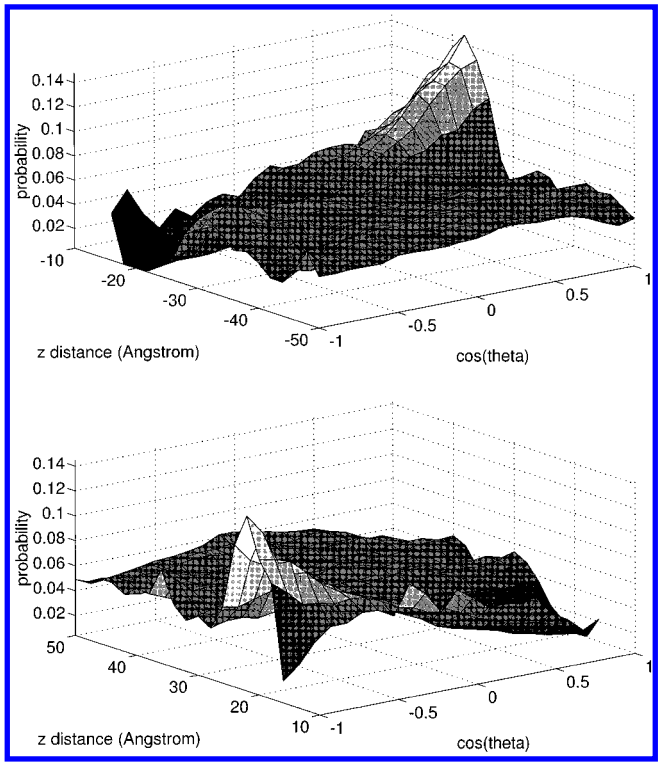

Figure 12. Probability distribution of the cosine of the angle theta as a function of the distance to the interface. θ is the angle between $\overrightarrow{8CH31O_k}$ vector and the interface normal.

half of its original neighbors. The $1O_k-2C_k$ RDF shows a first peak displacement of about 1 Å toward greater distances at the interface. That shift is the result of the hydrogen bridges established between the water hydrogens and the ketone oxygens, as will be confirmed in the next section. This association precludes dipole associations between the HPT2 molecules, resulting in a greater average distance between the $1O_k$ and $2C_k$ groups, which can be seen as a structural change in HPT2 caused by the presence of the aqueous phase. Those hydrogen bridges can also be found in bulk HPT2, although their statistical weight is negligible due to the small density of water in bulk HPT2.

5. HPT2 Orientational Structure. Figure 12 shows the probability distribution for the angle between the $\overrightarrow{8CH_31O_k}$ vector and the interface normal. In the bulk zone there are no preferred orientations. At the interface the HPT2 molecules show a clear tendency to become parallel to the interface normal, with the oxygen pointing into the aqueous phase, reflecting some amphiphilic behavior. The second molecular layer behind the interface also shows some tendency to be aligned parallel to the interface normal, although inverting the orientation (in this case the polar oxygens point toward the organic phase), to allow for the association between nonpolar carbon chains. This ordering tends to vanish as we progress into the organic phase and is almost negligible at the third molecular layer from the interface.

The interfacial bilayer structure of HPT2 can also be detected in a plot of the density of polar and organic terminal groups as a function of the distance to the interface. To this end, we divided the simulation box in slabs of 1 Å thickness parallel to the interfacial plane and computed the average number of $1O_k$ and $8CH_3$ sites in each slab.

In Figure 13 it can be seen that the number of HPT2 oxygens presents two peaks, one located at the interfacial zone and the other located two molecular diameters away from the interface.

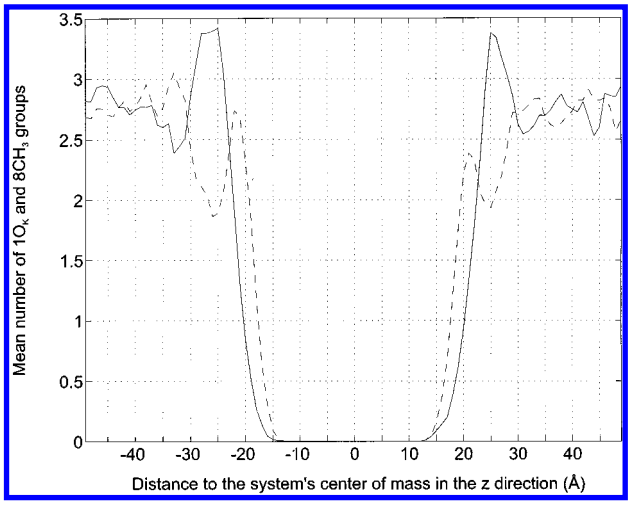

Figure 13. Average number of $8CH_3$ groups (solid line) and average number of $1O_k$ groups (dashed line) in each slab considered.

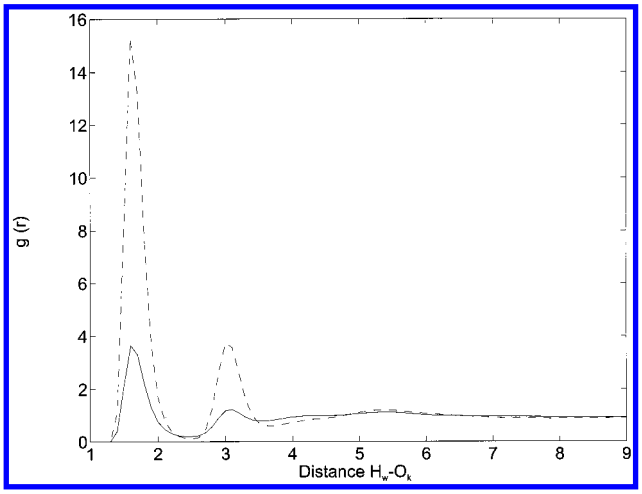

Figure 14. RDFs for the H_w-1O_k groups at the interface (solid line) and in bulk HPT2 (dashed line).

Between them a peak appears corresponding to the average number of chain terminal groups, as predictable from bilayer arrangement.

6. Degree of Molecular Folding. To explore the degree of HPT2 folding, the probability distribution for the distance between the $3CH_3$ and $8CH_3$ groups was computed in bulk and interfacial regions. The distributions are quite similar, presenting a maximum at 6.8 Å (bulk) and at 6.7 Å (interface), and an average distance of 6.5 Å (bulk) and 6.4 Å (interface). Thus the molecules seem to keep their degree of folding almost unaffected at the interface.

7. Water−HPT2 RDFs. In this section the molecular associations between water and HPT2 molecules in the interfacial region are explored to characterize the interfacial structure. Many RDFs between water and HPT2 groups were computed but we concluded that the unique well defined structure formed (revealed by an RDF peak) results from the association between the water hydrogens and the HPT2 oxygen. Stereochemical effects make difficult the association between the carbonyl carbon and the water oxygen (the carbonyl carbon is too hidden by the methyl groups). Figure 14 presents the calculated RDFs for the H_w-1O_k groups at the interface and in bulk HPT2.

The association between the H_w and $1O_k$ atoms is clear. The position of the peaks is the same in the bulk solution and at the interface, and quite close to the one of the H_w-O_w RDF. The peaks are more pronounced in bulk HPT2 because at the

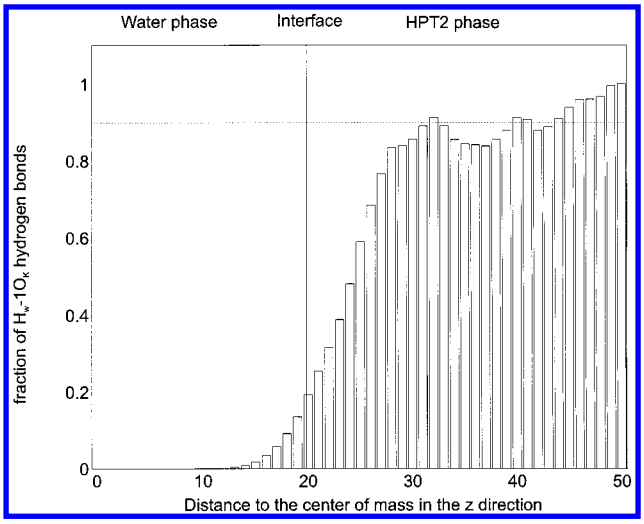

Figure 15. Fraction of H_w-1O_k hydrogen bonds in relation to the total number of hydrogen bonds. The dashed line locates the average fraction obtained in bulk HPT2.

interface the water proportion is larger than in bulk HPT2, and the association of hydrogens with the water oxygen is energetically more favorable than with the ketone oxygens. Integration of the first peaks results in an average of 0.84 $1O_k$ groups per water hydrogen in bulk HPT2 and 0.13 $1O_k$ groups per water hydrogen at the interface.

More details about the hydrogen bonding between water and HPT2 oxygens can be obtained from Figure 15. This figure displays the fraction of water hydrogens that are hydrogen bonded to ketone oxygens, in relation to the total number of hydrogen bonds, as a function of the distance to the interface.

At the Gibbs dividing surface, a fraction of 0.16 of the hydrogen bonds are made with the ketone oxygen. This number increases until 12 Å past the interface, where it converges to a value of 0.90. Again it can be seen that the water structure suffers little changes until the Gibbs dividing surface, and its most important transformations appear at the organic side of the interface.

D. Dynamics

1. Orientational Dynamics. The normalized time autocorrelation function for the molecular orientation was calculated according to the equation below:

$$C(\xi) = \langle \vec{v}(t)\vec{v}(t+\xi)\rangle_t / \langle \vec{v}(t)\vec{v}(t)\rangle_t \qquad (9)$$

where the brackets represent a mean over all time origins t.

The autocorrelation time for the orientation of the molecules was also estimated through

$$t_{corr} = \int_{\xi=0}^{\infty} C(\xi)\, d\xi \qquad (10)$$

Because the decay of the correlation functions is very slow, and because of block analysis, the functions have been computed until 10 ps only, and an exponential fit was made to estimate the value of the integral in equation 10 from 10 ps till infinity. This procedure was tested by comparing the results of the extrapolations with one estimation of the correlation function until 200 ps, using all data produced in a simulation, and it was checked that it was very accurate.

Figure 16 and Table 1 display the results obtained for the water dipole and the $\overrightarrow{HH}$ vectors. We plotted the ln $C^{1/2}(\xi)$ vs

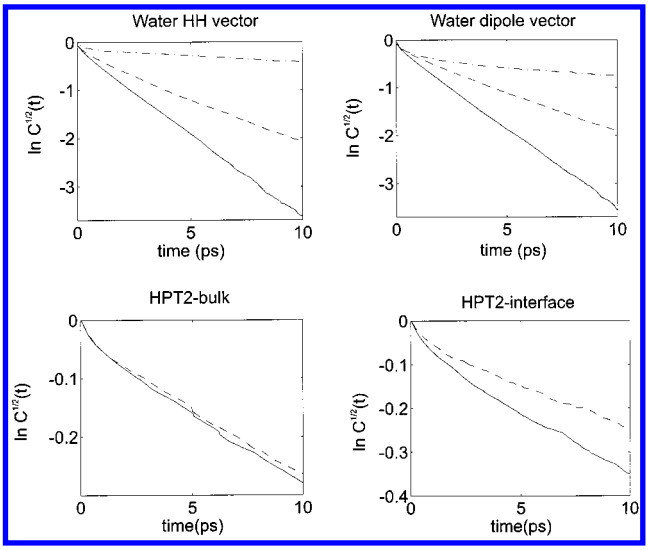

Figure 16. Semilogs of the orientational correlation functions for water and HPT2. In the top figures the solid lines correspond to bulk water, the dashed lines correspond to interfacial water and the dashed-dotted lines correspond to water in bulk HPT2. In the bottom figures, the solid lines correspond to reorientations parallel to the interfacial plane and the dashed lines correspond to reorientations normal to the interface.

TABLE 1: Orientational Correlation Times (Picoseconds)[a]

	bulk water	interface	bulk HPT2
water dipole	2.5 ± 0.1	4.7 ± 0.1	20 ± 2
$\overrightarrow{HH}$	2.4 ± 0.1	4.2 ± 0.1	32 ± 2
HPT2	not available	33 ± 1(∥), 48 ± 1(⊥)	39 ± 1

[a] Near the interface the HPT2 correlation times for reorientations parallel (∥) and perpendicular (⊥) to the interfacial plane were calculated separately.

ξ since several stochastic models for reorientation dynamics[30,31] predicted that this function should be proportional to $-\xi$.

As can be seen, for water, the approaching to the interface results in a slowing of the reorientational dynamics, which is consistent with the enhancement of hydrogen bonding at the interface. In bulk HPT2 the water rotation becomes coupled to the HPT2 rotation since almost all water molecules are hydrogen bonded to HPT2 molecules.

For the HPT2 molecules the normalized vector $\vec{v} = \overrightarrow{3CH_37CH_2}$ was considered as representative of the orientation of HPT2 molecules. We can see from Figure 16 and Table 1 that the HPT2 orientational dynamics becomes anisotropic at the interface, the reorientation parallel to the interfacial plane happening faster than the one normal to the interface. The shape and size of the water molecules presents less hindrance to the reorientation of the long HTP2 molecules, allowing a faster reorientation in the interfacial plane. However, rotations about an axis in the plane of the interface are constrained by the preferred interfacial orientation (perpendicular to the interfacial plane) which is stabilized by the hydrogen bonds between the ketone oxygen and the water hydrogens. This results in a slower orientational dynamics of $\vec{v}_z$ near the interface. In the bulk region the orientational dynamics was found to be isotropic.

2. Diffusion. The translational diffusion coefficients for the center of mass (com) of water and HPT2 were calculated according to the Einstein relation:

$$D = \lim_{t\to\infty} \frac{\Delta R^2}{6t} \qquad (11)$$

where D is the diffusion coefficient, ΔR is the com displacement, and t is the time.

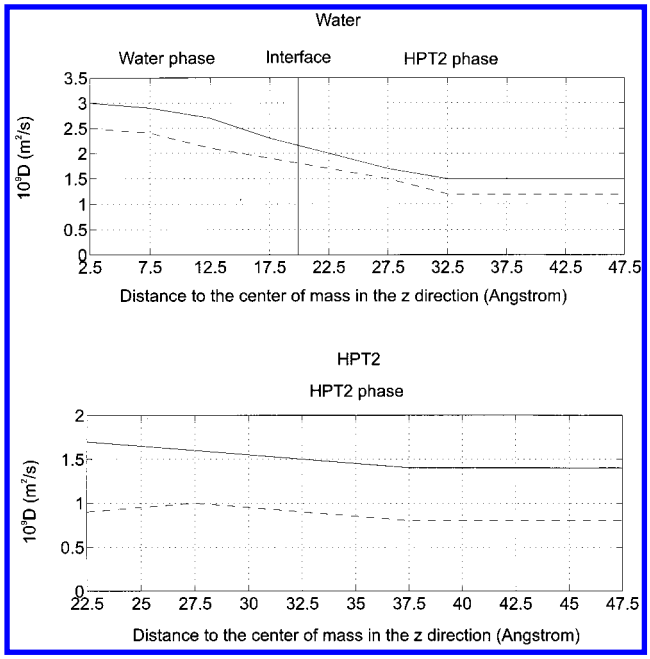

Figure 17. Diffusion coefficients for water (top) and HPT2 (bottom) as a function of the distance from the interface. Solid lines correspond to diffusion in the interfacial plane, and dashed lines correspond to diffusion perpendicular to the interface.

The box was divided into slabs of 5 Å of thickness. The diffusion coefficients were calculated in each slab. The z coordinate of every molecule was monitored in order to prevent accumulation of data from molecules which diffuse outside their initial slab during the interval $[t, t + \tau]$, where t is the time origin and τ the time increase, which is not greater than half the average residence time of the molecules in each slab. Figure 17 displays the results obtained.

We have estimated the error associated with the diffusion coefficients using the dispersion in the results obtained by the independent analysis of each half of the four simulations. For HPT2 we obtained a constant rms of $0.1.10^{-9}$ m^2 s^{-1}. In the case of water we obtained rms from $(0.06-0.08) \times 10^{-9}$ m^2 s^{-1} for slabs away from the interface to 0.2×10^{-9} m^2 s^{-1} for slabs in the organic phase (this last large value is due to the small number of molecules in the organic phase).

Water diffusion was found to be anisotropic in all extension of the simulation box, being slower towards the interface than parallel to it. Water molecules in bulk HPT2 present diffusion coefficients quite close to those of HTP2. The water molecules are strongly coupled to HPT2, via hydrogen bonds, and both molecules tend to move together. Concerning HPT2, we also observe that diffusion perpendicular to the interface is slower than diffusion in the interfacial plane. There is an enhancement of the anisotropic effect near the interface. Anisotropy along all the extension of the simulation box can also be found, to a larger or lesser extent, for other liquid−liquid interfacial systems.[14,15,32] Therefore, the existence of an interface imposes a long range effect under diffusion, and the simulation boxes traditionally used are not large enough to attain real bulk diffusion properties. However, the use of much bigger simulation boxes is not feasible with the current computer resources. In the present simulations the anisotropy in the diffusion is the effect which extends the farthest away from the interface.

3. Life Time of the Water Hydrogen Bonds. In order to evaluate the effect of the interface on the stability of the water hydrogen bonds (Hbs), we computed the probability distribution of the life time of the Hbs, which was considered to be the time elapsed since the formation of the Hb until the first time that the H_w-O_w distance exceeds the first minima in the H_w-O_w RDF. Both distributions obtained are very broad and quite similar, being the interfacial Hbs more stable than the bulk ones (see Figure 18).

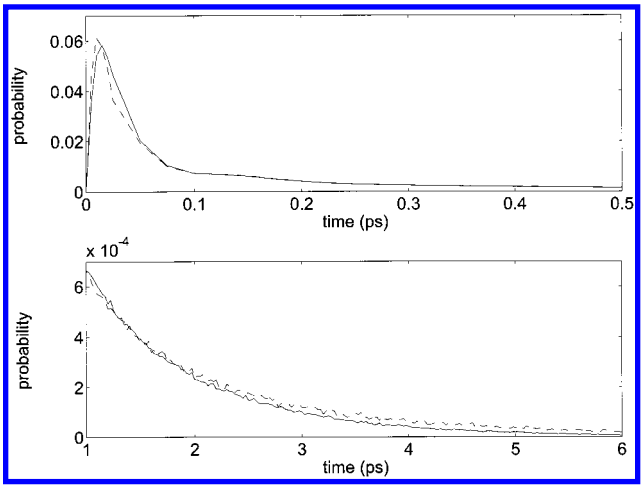

Figure 18. Probability distribution of the life time of the water hydrogen bonds. Solid lines correspond to bulk water and dashed lines to interfacial water.

From the distributions depicted in Figure 12 the mean life time was found to be 0.44 ps in the bulk region and 0.56 ps at the interface, which corresponds to an increase of 27%. This is consistent with the conservation of the water structure near the interface, the difference observed being due to the smaller number of molecules inside the first coordination shell (−24%). So, if we take the total lifetime of the Hbs for a central molecule as the mean lifetime of their Hbs times the average number of Hbs that the central molecule establishes

$$\text{Time}_{\text{total}}\text{Hbs} = \langle \text{life time Hbs} \rangle \langle \text{number Hbs} \rangle \qquad (12)$$

we will conclude that this quantity remains almost unchanged in the bulk region and at the interface.[33] The water molecules do not have so many neighbors in competition to establish Hbs, resulting in a longer life for each Hb.

IV. Conclusions

The water|HPT2 interface was found to be molecularly sharp and very corrugated by capillary waves. The HPT2 molecules in direct contact with water point their polar heads towards the aqueous phase and point the nonpolar chain into the bulk organic phase. The second HPT2 molecular layer reverses this orientation, forming a bilayer structure. This ordering tends to vanish as we progress into the organic phase, and is almost negligible at the third molecular layer. At the interface, hydrogen bonds between the water hydrogen and the ketone oxygen are formed. This stable association supports the existence of a very thick mixed region, where water penetrates into the hydrophilic HPT2 head-groups region but not into the hydrophobic core. Earlier simulations of liquid−liquid interfaces did not reveal significant aqueous−organic pair correlations at the interface, which might be due to the greater hydrophobicity of the organic solvents used.

It seems that interfacial sharpness is a common pattern in water/organic liquid/liquid interfaces, regardless of the organic solvent used. This is the case for several systems, from the highly hydrophobic water/decane interface to the slightly hydrophilic water/HPT2 interface. As far as we know the

reverse situation (a broad interface, with a gradual composition change) has never been found in computer simulated systems.

The water structure is only slightly affected by the presence of the organic phase, and important changes only occur in the organic side of the interface. Near the interface the water molecules show a preference in having their dipole vectors parallel to the interfacial plane. This ordering extents through 2 or 3 molecular layers into the aqueous phase. In the aqueous side of the interface, the water dipoles point slightly to the water phase and in the other side they point slightly to the organic phase, to allow the formation of Hbs between water and the ketone oxygen. The water coordination shell remains stable at the interface, showing only a small decrease in its coordination number (5.2 to 4.2). Because the density of water at the interface is only one-half of the bulk one, the robustness of the water structure becomes evident. As water progresses into the organic phase its coordination number decreases until an average of 0.7 neighbors in bulk HPT2.

The HPT2 structure is not so resistant. On average, the interfacial coordination number of HPT2 decreases to one-half of the bulk value, reflecting the decrease to one-half on the density of HPT2 at the interface. Dipole associations between HPT2 molecules become more restricted due to the formation of hydrogen bonds with water.

The self-diffusion of both liquids was found to be anisotropic along all extension of the simulation box, being that diffusion toward the interface is slower than that parallel to the interfacial plane. This seems to be the longest range interfacial effect induced by the interface. Much larger simulation boxes would be necessary to estimate the amplitude of this effect.

Reorientation dynamics of water becomes slower at the interface, which is consistent with the enhancement of hydrogen bonding. In the case of HTP2, reorientation in the interfacial plane becomes faster at the interface. The shape and size of the water molecules present a lower hindrance to the rotation of the long HPT2 molecules. Reorientations in a plane perpendicular to the interface are slower near the interface, because of the hydrogen bonds established between the water hydrogens and the ketone oxygen. Large angular displacements perpendicular to the interface would destroy those structures and are not energetically favorable. Exchanges concerning the orientational dynamics are limited to the interfacial zone.

Acknowledgment. Financial support from Fundação para a Ciência e a Tecnologia (Lisbon) through PRAXIS/PCEX/QUI/61/96 is acknowledged. P.A.F. thanks the Programa Praxis XXI for a doctoral scholarship (BD/9175/96). Helpful discussions with Prof. A. Fernando Silva and Mr. Alfredo J. P. Carvalho of this department are gratefully acknowledged.

References and Notes

(1) Honig, B. H.; Hubbell, W. L.; Flewelling, R. F. *Ann. Rev. Biophys. Chem.* **1986**, *15*, 163.
(2) Arai, K.; Ohsawa, M.; Kusu, F.; Takamura, K. *Bioelectrochem. Bioenerg.* **1993**, *31*, 65.
(3) Cunnane, V. J.; Schiffrin, D. J.; Beltran, C.; Geblewicz, G.; Solomon, T. *J. Electroanal. Chem.* **1988**, *247*, 203.
(4) Koryta, J.; Skalicky, M. *J. Electroanal. Chem.* **1987**, *229*, 265.
(5) *The Interface Structure and Electrochemical Processes at the Boundary Between two Immiscible Liquids*; Kazarinov, V. E., Ed.; Springer: Berlin, 1987.
(6) Tomasi, J.; Persico, M. *Chem. Rev.* **1994**, *94*, 2027.
(7) Higgins, D. A.; Corn, R. M. *J. Phys. Chem.* **1993**, *97*, 489.
(8) Grubb, S. C.; Kim, M. W.; Rasing, T.; Shen, Y. R. *Langmuir* **1988**, *4*, 452.
(9) Conboy, J. C.; Daschbach, J. L.; Richmond, G. L. *J. Phys. Chem.* **1994**, *98*, 9688.
(10) Du, Q.; Superfine, R.; Freysz, E.; Shen, Y. R. *Phys. Rev. Lett.* **1993**, *70*, 2313.
(11) Eisenthal, K. B. *Annu. Rev. Phys. Chem.* **1992**, *43*, 627.
(12) Lynse, P. *J. Chem. Phys.* **1987**, *86*, 4177.
(13) Gao, J.; Jorgensen, W. *J. Phys. Chem.* **1988**, *92*, 5813.
(14) Benjamin, I. *J. Chem. Phys.* **1992**, *97*, 1432.
(15) Michael, D.; Benjamin, I. *J. Phys. Chem.* **1995**, *99*, 1530.
(16) Chang, T.; Dang, L. X. *J. Chem. Phys.* **1996**, *104*, 6772.
(17) Cheng, Y.; Schiffrin, D. *J. Electroanal. Chem.* **1996**, *409*, 9.
(18) Cheng, Y.; Schiffrin, D. *J. Electroanal. Chem.* **1997**, *429*, 37.
(19) Fernandes, P. A.; Cordeiro, M. N. D. S.; Gomes, J. A. N. F. *J. Phys. Chem. B* **1999**, *103*, 1176.
(20) Berendsen, H. J. C.; Grigera, J. R.; Straatsma, T. P. *J. Phys. Chem.* **1987**, *91*, 6269.
(21) Jorgensen, W. L.; Tirado-Rives, J. *J. Am. Chem. Soc.* **1988**, *110*, 1657.
(22) Brooks, B. B.; Bruccolery, R. E.; Olafson, B. D.; States, D. J.; Swaminathan, S.; Karplus, M. J. *J. Comput. Chem.* **1983**, *4*, 187.
(23) Hoover, W. *G. Phys. Rev.* **1985**, *A31*, 1695.
(24) Melchionna, S.; Ciccotti, G.; Holian, B. L. *Mol. Phys.* **1993**, *78*, 533.
(25) Forrester, T. W.; Smith, W. *Mol. Simul.* **1994**, *13*, 195.
(26) Weeks, J. D. *J. Chem. Phys.* **1977**, *67*, 3106.
(27) Perkus, J. K.; Williams, G. O. *Fluid Interfacial Phenomena*; Wiley: New York, 1986.
(28) Weast, R. C., Ed. *Handbook of Chemistry and Physics*; CRC Press: Boca Raton, FL, 1989.
(29) Wilson, M. A.; Pohorrille, A.; Pratt, L. *J. Phys. Chem.* **1987**, *91*, 4873.
(30) Steele, W. A. *Adv. Chem. Phys.* **1976**, *34*, 1.
(31) Barnes, A. J., Orville-Thomas, W. L., Yarwood, J., Eds.; *Molecular Liquids Dynamics and Interactions*; Reidel: Dordrecht, 1984.
(32) Schweighofer, K. J.; Benjamin, I. *J. Electroanal. Chem.* **1995**, *391*, 1.
(33) The average number of hydrogen bonds per water molecule can be taken from Figure 8 as 3.65 for the bulk water molecules and 3.06 for the interfacial water molecules.